

Amyloid β -Binding Bifunctional Chelators with Favorable Lipophilicity for ^{64}Cu Positron Emission Tomography Imaging in Alzheimer's Disease

Juyue Wang, Truc T. Huynh, Hong-Jun Cho, Yung-Ching Wang, Buck E. Rogers,* and Liviu M. Mirica*

Cite This: *Inorg. Chem.* 2021, 60, 12610–12620

Read Online

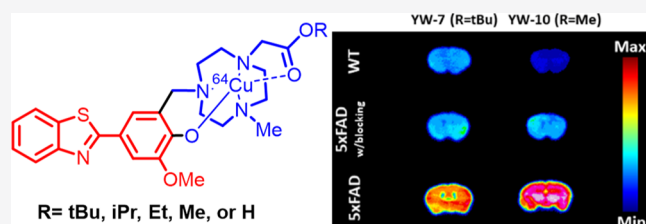
ACCESS |

Metrics & More

Article Recommendations

Supporting Information

ABSTRACT: Herein, we report a new series of bifunctional chelators (BFCs) with a high affinity for amyloid aggregates, a strong binding affinity toward Cu(II), and favorable lipophilicity for potential blood–brain barrier penetration. The alkyl carboxylate ester pendant arms offer up to 3 orders of magnitude higher binding affinity toward Cu(II) and enable the BFCs to form stable ^{64}Cu -radiolabeled complexes. Among the five compounds tested, the ^{64}Cu -YW-7 and ^{64}Cu -YW-10 complexes exhibit strong and specific staining of amyloid plaques in ex vivo autoradiography studies. Importantly, these BFCs have promising partition coefficient ($\log D_{\text{oct}}$) values of 0.91–1.26 and show some brain uptake in biodistribution studies using CD-1 mice. Overall, these BFCs could serve as lead compounds for the development of positron emission tomography imaging agents for AD diagnosis.



INTRODUCTION

Alzheimer's disease (AD) is a progressive neurodegenerative disease and the most prevalent form of dementia. The progression of AD leads to synaptic failure and neuronal death, resulting in cognitive decline in memory, learning skill, and language.^{1,2} The brains of AD patients are characterized by the deposition of senile plaques composed of the aggregates of amyloid β ($A\beta$). $A\beta$ peptides are derived from the amyloid precursor protein, and the main $A\beta$ peptides are 42 and 40 amino acids long.^{3–7}

To date, there has been no cure for AD, and the current treatments only alleviate the symptoms and are not able to modify the pathological progression of AD.⁸ The early diagnosis of AD could contribute to a better preparation of intervention and care plan, and to improve the life quality of patients. Molecular imaging modalities such as positron emission tomography (PET) allow for noninvasive assessment of the $A\beta$ burden in patients. Pittsburgh compound B (^{11}C -PiB) is the most extensively used amyloid PET imaging agent, but its clinical usage is greatly limited by a short half-life (20 min) of ^{11}C .⁹ In comparison, ^{18}F is a more suitable radioisotope with a longer half-life of 109.8 min. To date, three compounds have been approved by the US Food and Drug Administration (FDA) for amyloid imaging: the benzothiazole derivative ^{18}F -flutemetamol (Vizamyl), and the stilbene derivatives ^{18}F -florbetaben (Neuraceq) and ^{18}F -florbetapir (Amyvid).^{10–12}

However, the relative short half-lives and the necessity of covalent incorporation of the ^{11}C and ^{18}F radionuclides have limited the widespread clinical usage of these imaging probes.¹³ By comparison, the radionuclide ^{64}Cu has a longer

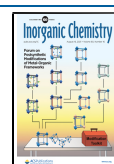
half-life of 12.7 h, and its well-established coordination chemistry allows for easy conjugation with the biologically relevant molecules.^{14–16} Thus, ^{64}Cu PET imaging agents containing amyloid-targeting fragments could assist in early diagnosis of AD, monitoring in vivo response to therapy, and greatly facilitating the development of therapeutics for AD.^{3,17–26}

For PET imaging purposes, a chelator that forms highly stable ^{64}Cu complexes is critical for minimizing unspecific tissue uptake. 1,4,7-Triazacyclononane (TACN)-based ligands have been extensively studied as copper chelating agents, including radiotracers for molecular imaging.²⁷ Chelators that contain the 1,4,7-triazacyclononane-1,4,7-triacetic acid (NOTA) ligands have shown the formation of stable ^{64}Cu -complexes in vivo. The acetic acid arms of the TACN backbone were proposed to enhance the complexation with the metal ion by forming a hexadentate ligand that is known to form the ^{64}Cu complexes that are stable in vitro and in vivo.²⁸

Nevertheless, the presence of several free carboxylic acid groups in these chelators limits their blood–brain barrier (BBB) permeability, which is usually the biggest limiting factor for imaging agents targeting the central nervous system.^{29,30}

Received: July 8, 2021

Published: August 5, 2021



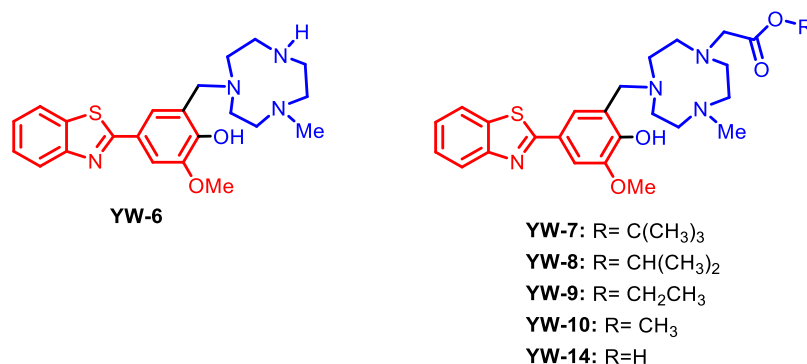


Figure 1. Structures of the ligands investigated herein. The metal-binding and $\beta 5$ -interacting fragments are shown in blue and red, respectively.

Thus, herein, we employ the strategy of using the ester derivatives of the carboxylate pendant arm attached to the TACN backbone (Figure 1), in order to increase the lipophilicity of the bifunctional chelators (BFCs) and facilitate brain uptake. The additional O donor atoms from the ester arm should also lead to the formation of metal complexes with greater stability in vivo. Inspired by the imaging probes mentioned above, our purpose is to design ester-based ⁶⁴Cu PET imaging agents that target the $\beta 5$ species and could be potentially used as AD diagnostics.

EXPERIMENTAL SECTION

General Methods. All reagents were purchased from commercial sources and used as received unless stated otherwise. 1-Methyl-1,4,7-triazacyclononane (MeH₃tacn) was synthesized according to the reported procedures.³¹ All solutions and buffers were prepared using metal-free Millipore water that was treated with Chelex overnight and filtered through a 0.22 μ m nylon filter. ¹H (300 MHz) NMR spectra were recorded on a Varian Mercury-300 spectrometer or a VARIAN UNITY Inova 400 spectrometer. ¹³C (126 MHz) NMR spectra were recorded on a VARIAN VXR 500 with UNITY INOVA Console spectrometer. Chemical shifts are reported in parts per million and referenced to residual solvent resonance peaks. UV–visible spectra were recorded on a Varian Cary 50 Bio spectrophotometer and are reported as λ_{max} nm (ϵ , M⁻¹ cm⁻¹). All fluorescence measurements were performed using a SpectraMax M2e plate reader (Molecular Devices). EPR spectra were recorded on a Bruker 10" EMXPlus X-band Continuous Wave EPR spectrometer at 77 K. EPR spectral simulation and analysis were performed using the Bruker WINEPR SimFonia program, version 1.25. ESI-MS experiments were performed by the Mass Spectrometry Lab at UIUC using a Waters Q-TOF Ultima ESI mass spectrometer with an electron spray ionization source. Colocalization analysis and determination of the Pearson's correlation coefficient were performed with the imaging software Fiji (ImageJ 1.52p).

Synthesis of BFCs. **YW-7.** To a suspension of YW-6 (100 mg, 0.24 mmol) and sodium carbonate (28 mg, 0.26 mmol) in MeCN (15 mL), *tert*-butyl bromoacetate (52 mg, 0.26 mmol) in MeCN (5 mL) was added. The reaction mixture was stirred at room temperature for 12 h. The solvent was removed to give an orange-yellow residue that was purified by Combi-Flash (reverse-phase) using MeCN/H₂O/trifluoroacetic acid (TFA) (40:60:0.1) to yield a yellow solution, which was then neutralized with NaHCO₃, extracted with dichloromethane, and dried to give a yellow solid (118 mg, yield 93%). ¹H NMR (400 MHz, CDCl₃): δ 7.98 (d, *J* = 8.1 Hz, 1H), 7.83 (d, *J* = 7.9 Hz, 1H), 7.56 (s, 1H), 7.48–7.38 (m, 2H), 7.32 (t, *J* = 8.1 Hz, 1H), 3.92 (d, *J* = 26.6 Hz, 5H), 3.25 (s, 6H), 2.98 (s, 4H), 2.82 (s, 3H), 2.68 (d, *J* = 21.8 Hz, 4H), 1.39 (s, 9H). ¹³C NMR (126 MHz, CDCl₃): δ 171.49, 168.34, 154.39, 148.54, 135.00, 126.48, 125.03, 123.87, 122.93, 121.73, 110.06, 56.55, 29.95, 28.41. HR-ESI-MS: calcd for [M + H]⁺, 527.2647; found, 527.2680.

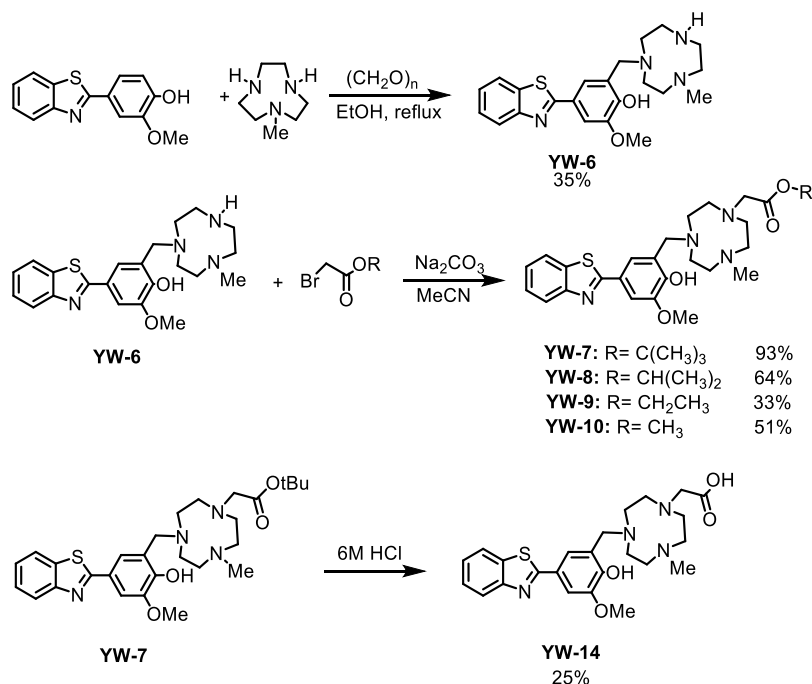
YW-8. To a suspension of YW-6 (20 mg, 0.05 mmol) and sodium carbonate (6 mg, 0.05 mmol) in MeCN (5 mL), *iso*-propyl bromoacetate (10 mg, 0.05 mmol) in MeCN (5 mL) was added. The reaction mixture was stirred at room temperature for 24 h. The solvent was removed to give a yellow residue that was purified by Combi-Flash (reverse-phase) using MeCN/H₂O/TFA (45:55:0.1) to yield a yellow solution, which was then neutralized with NaHCO₃, extracted with dichloromethane, and dried to give a yellow solid (16 mg, yield 64%). ¹H NMR (300 MHz, CDCl₃): δ 8.01 (d, *J* = 9.3 Hz, 1H), 7.87 (d, *J* = 9.2 Hz, 1H), 7.61 (s, 1H), 7.53–7.42 (m, 2H), 7.41–7.31 (m, 1H), 4.98 (p, *J* = 6.2 Hz, 1H), 4.02 (s, 5H), 3.39 (s, 4H), 3.06 (s, 4H), 2.90 (s, 3H), 2.73 (s, 4H), 1.21 (d, *J* = 6.3 Hz, 5H). ¹³C NMR (126 MHz, CDCl₃): δ 171.91, 168.53, 134.97, 126.44, 124.95, 123.53, 122.88, 121.71, 110.01, 68.29, 58.41, 57.27, 56.48, 29.95, 22.18. HR-ESI-MS: calcd for [M + H]⁺, 513.2491; found, 513.2500.

YW-9. To a suspension of YW-6 (36 mg, 0.09 mmol) and sodium carbonate (9 mg, 0.09 mmol) in MeCN (10 mL), ethyl bromoacetate (52 mg, 0.26 mmol) in MeCN (5 mL) was added. The reaction mixture was stirred at room temperature for 12 h. The solvent was removed to give an orange-yellow residue that was purified by Combi-Flash (reverse-phase) using MeCN/H₂O/TFA (50:50:0.1) to yield a yellow solution, which was then neutralized with NaHCO₃, extracted with dichloromethane, and dried to give a yellow solid (14 mg, yield 33%). ¹H NMR (300 MHz, CDCl₃): δ 8.00 (d, *J* = 8.6 Hz, 1H), 7.86 (d, *J* = 8.6 Hz, 1H), 7.57 (s, 1H), 7.50–7.42 (m, 1H), 7.40 (d, *J* = 2.0 Hz, 1H), 7.37–7.30 (m, 1H), 4.12 (q, *J* = 7.1 Hz, 2H), 4.00 (s, 3H), 3.92 (s, 2H), 3.13–2.73 (m, 12H), 2.66 (s, 3H), 1.38–1.14 (m, 6H). ¹³C NMR (126 MHz, CDCl₃): δ 172.17, 154.38, 148.61, 134.99, 130.50, 127.29, 126.47, 125.02, 122.91, 121.73, 110.10, 63.04, 60.75, 60.21, 56.53, 52.95, 29.95, 14.48. HR-ESI-MS: calcd for [M + H]⁺, 499.2334; found, 499.2319.

YW-10. To a suspension of YW-6 (25 mg, 0.06 mmol) and sodium carbonate (28 mg, 0.26 mmol) in MeCN (15 mL), *tert*-butyl bromoacetate (52 mg, 0.26 mmol) in MeCN (5 mL) was added. The reaction mixture was stirred at room temperature for 16 h. The solvent was removed to give an orange-yellow residue that was purified by Combi-Flash (reverse-phase) using MeCN/H₂O/TFA (45:55:0.1) to yield a yellow solution, which was then neutralized with NaHCO₃, extracted with dichloromethane, and dried to give a yellow solid (15 mg, yield 51%). ¹H NMR (300 MHz, CDCl₃): δ 8.00 (d, *J* = 9.2 Hz, 1H), 7.86 (d, *J* = 8.5 Hz, 1H), 7.57 (s, 1H), 7.51–7.41 (m, 1H), 7.35 (dd, *J* = 16.8, 8.3 Hz, 2H), 3.99 (s, 3H), 3.92 (s, 2H), 3.66 (s, 3H), 3.11–2.73 (m, 12H), 2.64 (s, 3H). ¹³C NMR (126 MHz, CDCl₃): δ 172.95, 168.72, 151.65, 148.8, 126.38, 124.84, 122.84, 121.68, 120.88, 110.03, 60.78, 58.47, 56.43, 55.87, 53.68, 46.68, 29.95. HR-ESI-MS: calcd for [M + H]⁺, 485.2778; found, 485.2794.

YW-14. The ester YW-7 (50 mg, 95 μ mol) was dissolved in 10 mL of 6 M HCl and stirred at room temperature for 24 h. The solvent was removed to get a yellow residue, which was dissolved in diethyl ether and filtered. Removal of the solvent gave a light-yellow powder, which was dried under vacuum to obtain the product (11 mg, yield 25%).

Scheme 1. Syntheses of BFCs



¹H NMR (499 MHz, CD₃OD) δ 8.47 (s, 1H), 8.13 (dd, $J = 29.6, 8.1$ Hz, 2H), 7.97 (s, 1H), 7.67 (dt, $J = 48.7, 7.3$ Hz, 2H), 4.09 (s, 4H), 4.01 (s, 2H), 3.63–3.29 (m, 12H), 3.08 (s, 3H). ¹³C NMR (126 MHz, CD₃OD) δ 172.59, 153.19, 149.21, 129.33, 127.82, 123.47, 111.71, 56.65, 54.76, 50.68. HR-ESI-MS: calcd for [M + H]⁺, 471.2021; found, 471.2058.

Acidity and Stability Constant Determination. UV–vis pH titrations were employed for the determination of acidity constants of BFCs and stability constants with Cu(II). For acidity constants, solutions of ligands **YW-6** to **YW-10** (20 μ M, 0.1 M NaCl, pH 3) were titrated with small aliquots of 0.1 M NaOH, and **YW-14** (20 μ M, 0.1 M NaCl, pH 1.2) was titrated with small aliquots of 1 M NaOH at room temperature under a steady moist flow of N₂. At least 30 UV–vis spectra were collected in the pH 1.2–11 range. Dimethyl sulfoxide (DMSO) stocks (10 mM) were diluted in a MeOH–water mixture in which MeOH did not exceed 1% (v/v). Similarly, stability constants were determined by titrating solutions of **YW-6** and 1 equiv of Cu(ClO₄)₂·6H₂O (20 μ M) with small aliquots of 0.1 M NaOH, and **YW-7** to **YW-10** and 0.9 equiv of Cu(ClO₄)₂·6H₂O (18 μ M) with small aliquots of 0.2 M NaOH at room temperature. A solution of **YW-14** and 0.9 equiv of Cu(ClO₄)₂·6H₂O (18 μ M) was titrated with small aliquots of 1 M NaOH, and at least 30 UV–vis spectra were collected in the pH 1.2–11 range. The acidity and stability constants were calculated using the HypSpec computer program (Protonic Software, UK).³² Speciation plots of the compounds and their metal complexes were calculated using the program HySS2009 (Protonic Software, UK).³³

Histological Staining of 5xFAD Mouse Brain Sections. Eleven month old 5xFAD mouse brain sections were blocked with bovine serum albumin [2% BSA in phosphate-buffered saline (PBS), pH 7.4, 10 min] and treated with 50 μ M PBS solutions of BFCs or their Cu(II) complexes for 30 min, followed by treatment with a 2 μ M Congo Red solution for 30 min. The sections were treated with BSA again (4 min) to remove any compound nonspecifically bound to the tissue. Finally, the sections were washed with PBS (3 \times 2 min), deionized water (2 min), and mounted with nonfluorescent mounting media. For antibody staining, six month old 5xFAD mouse brain sections were treated with 50 μ M PBS solutions of BFCs or their Cu(II) complexes at room temperature for 1 h, followed by incubation with the AF594-conjugated anti-A β antibody (AF594-HJ3.4 antibody)^{34,35} solution (1 μ g/mL) for 1 h. The stained brain

sections were imaged using a Zeiss LSM 7010 confocal fluorescent microscope and Invitrogen EVOS FL Auto 2 Imaging System (Thermo Fisher, USA). Excitation and emission wavelengths of DAPI channel and Texas Red channel are $\lambda_{\text{ex}} = 357$ nm, $\lambda_{\text{em}} = 447$ nm, and $\lambda_{\text{ex}} = 585$ nm, $\lambda_{\text{em}} = 628$ nm, respectively.

Job's Plots for Solution Stoichiometry Determination. To determine the ligand/Cu stoichiometry for BFC, stock solutions (500 μ M) of BFC and CuCl₂·2H₂O (500 μ M) were prepared in DMSO and the spectra were measured using a Cary Bio UV–vis instrument. Each ligand has the same metal binding motif, therefore each ligand is assumed to bind to Cu(II) in a similar manner. Solutions containing different ratios of ligand and Cu ions were recorded from 0 to 100 mol % Cu (total concentration = 25 μ M). Appropriate amounts of the stock solutions were dissolved into 500 μ L of PBS pH 7.4 buffer and allowed to equilibrate for 5 min before recording the spectra.

Radiolabeling Studies. ⁶⁴Cu was produced by a (p,n) reaction on enriched ⁶⁴Ni on a TR-19 biomedical cyclotron (Cyclotron Corporation, Berkeley, CA) at Mallinckrodt Institute of Radiology, Washington University School of Medicine, and purified with an automated system using standard procedures.^{36,37} The BFCs were stored as DMSO stocks. The compounds were diluted to get a concentration of 1 mM. 20 μ L of the BFC solution was added to 100 μ L of 0.1 M NH₄OAc (pH 5.5), followed by the addition of 7.4 MBq (200 μ Ci) of ⁶⁴Cu stock solution. Various conditions (temperatures, pH, and reaction times) were attempted to optimize the labeling efficiency. For **YW-7**, **YW-10**, and **YW-14**, the solution was incubated at 45 $^{\circ}$ C for 1 h. For **YW-8** and **YW-9**, the solution was incubated at 80 $^{\circ}$ C for 2 h. Radiolabeled compounds were analyzed by HPLC in the mobile phase of water (0.1% TFA) and acetonitrile (0.1% TFA) with a gradient of 0–100% acetonitrile over 12 min and a flow rate of 1 mL/min. No further purification was needed if the ⁶⁴Cu-labeled complexes were obtained in a high radiochemical yield (>95%).

Lipophilicity Studies. Ten replicate Eppendorf tubes of 1:1 (v/v) *n*-octanol and PBS 1 \times were prepared (500 μ L each). The ⁶⁴Cu-labeled complexes (0.37 MBq, 10 μ Ci) were added to each tube, vortexed, and incubated in a thermomixer at 1000 rpm for 1 h. After 1 h, the solution was kept without shaking for 30 min to allow for the separation of the two layers. Aliquots (100 μ L) from the aqueous and the *n*-octanol layers were removed and counted separately in an automated gamma counter. Log *D*_{oct} values were obtained as the logarithms of the ratio of (activity detected in *n*-octanol)/(activity

detected in the aqueous layer). The overall average was recorded as the final log D_{oct} value for each compound. High log D_{oct} (1–2.5) is desired as it indicates the ability of radiolabeled products in crossing the BBB and reaching acceptable concentrations for brain imaging applications.³⁸

Biodistribution Studies. All animal experiments were performed in compliance with the Guidelines for Care and Use of Research Animals established by the Division of Comparative Medicine and the Animal Studies Committee of Washington University School of Medicine. Initial biodistribution studies were conducted in CD-1 female mice (Charles River Laboratories) of 5–7 weeks age. The injection dose was prepared by diluting into a 90% saline solution. The mice were injected via tail vein with 0.22–0.37 MBq (6–10 μ Ci) of each compound per animal in 100 μ L saline solution. After each time point (2, 60, and 240 min), mice were anesthetized with 1–2% isoflurane and euthanized by cervical dislocation. Brain, blood, kidney, liver, and other organs of interest were harvested and the amount of radioactivity in each organ was counted on a gamma counter containing a NaI crystal. The data were corrected for radioactive decay and percent injected dose per gram (% ID/g) of tissue was calculated. All samples were calibrated against a known standard. Quantitative data were processed by Prism 8 (GraphPad Software, v 6.03, La Jolla, CA) and expressed as mean \pm SD. Statistical analysis was performed using one-way analysis of variance and Student's *t*-test. Differences at the 95% confidence level ($p < 0.05$) were considered statistically significant.

Ex Vivo Autoradiography Studies. Brain sections of 11 month old 5xFAD transgenic mice and aged-matched wild type (WT) mice were obtained as described previously and immersed into a cryoprotectant solution. These sections were sorted and carefully removed using phosphate buffer in saline (PBS) to a 12-well plate. Each brain section was washed with 100% PBS three times, and \sim 0.925 MBq (25 μ Ci) of 64 Cu-labeled BFC in 2.5 mL PBS was added to completely cover the brain section and incubated for 1 h at room temperature in a shielded bunker. For blocking studies, 2-(4-hydroxyphenyl)benzothiazole (B₁) (Figure S37) was added to evaluate the specific binding of radiolabeled compounds.³⁹ After the incubation, brain sections (WT, 5xFAD, 5xFAD with blocking) were washed once with 1:1 (v/v) ethanol/PBS and then twice with PBS for 10 min of each washing cycle. Brain sections were removed, mounted onto microscopic slides, and briefly air-dried. The imaging slides were then mounted onto a phosphor imaging screen plate (GE Healthcare Life Sciences), and exposed overnight at -20 °C. The plates were scanned using a phosphor imager plate scanner (Storm 840) and the resulting images were processed using ImageJ (v1.48, public domain) software.

RESULTS AND DISCUSSION

Design and Syntheses of BFCs. The BFCs discussed herein are constructed by linking the $A\beta$ -binding fragment 2-(4-OH-phenyl)-benzothiazole with the metal-chelating TACN ligand via the Mannich reaction with paraformaldehyde (Scheme 1). The amyloid-targeting motif was generated by the condensation of 2-aminothiophenol with vanillin, followed by oxidation with atmospheric oxygen (Scheme S1). This fragment is derived from thioflavin T (ThT), a well-known amyloid-binding fluorescent dye, which shows a high binding affinity toward $A\beta$ species,⁴⁰ and that has been utilized as the amyloid-targeting motif in multifunctional compounds for PET imaging and treatment of AD.^{19–21,41–43}

To further enhance the metal chelation ability of BFCs, the pendant carboxylate arms were added to the TACN backbone by reacting YW-6 with a series of alkyl-bromoacetates, generating final products YW-7 to YW-10 that contain *tert*-butyl, *iso*-propyl, ethyl, and methyl ester groups, respectively. Hydrolysis of YW-7 in the presence of concentrated hydrochloric acid generates YW-14, which is a carboxylic acid and

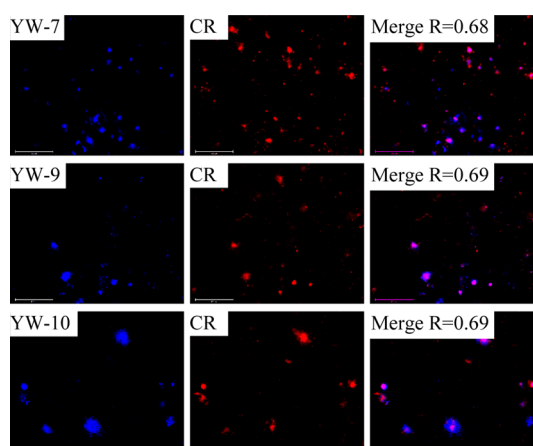


Figure 2. Fluorescence microscopy images of 5xFAD mouse brain sections incubated with compounds YW-7, YW-9, and YW-10 (left panels), Congo Red (middle panels), and merged images (right panels). The fluorescence signals from the BFCs and Congo Red were monitored at 447 and 628 nm upon excitation at 357 and 585 nm, respectively. Magnification: 20 \times . Scale bar: 125 μ m.

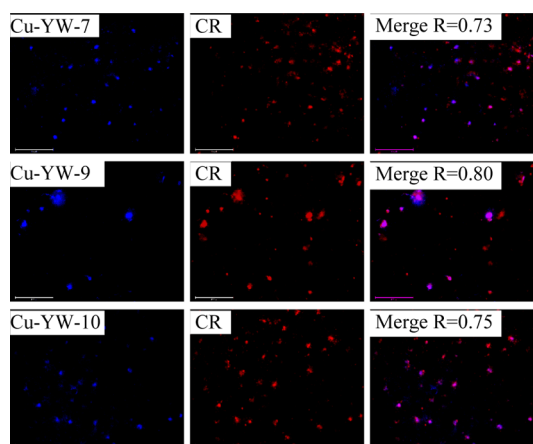


Figure 3. Fluorescence microscopy images of 5xFAD mouse brain sections incubated with Cu(II) complexes of YW-7, YW-9, and YW-10 (left panels), Congo Red (middle panels), and merged images (right panels). The fluorescence signals from the Cu(II) complexes and Congo Red were monitored at 447 and 628 nm upon excitation at 357 and 585 nm, respectively. Magnification: 20 \times . Scale bar: 125 μ m.

has the lowest molecular weight (<500 Da) among the BFCs, beneficial for the penetration of BBB according to Lipinski's rules.⁴⁴

UV–vis absorption spectra were acquired to determine the maximum UV–vis absorbance wavelength (λ_{abs}) of the BFCs and their Cu(II) complexes in PBS (pH = 7.4) buffer (Figures S1 and S2). Based on the UV–vis absorbance spectra, excitation wavelengths (λ_{ex}) of 328–332 nm (for BFCs) and 349 nm (for Cu(II) complexes) were used to examine their fluorescent properties (Figures S3 and S4). In the absorbance spectra of YW-7, YW-9, and YW-14, there is a \sim 20 nm red shift of absorbance peak maxima upon chelation with Cu(II). Due to the quenching effect by Cu(II), the fluorescence intensities of ester BFCs decrease by 3–4 fold, while that of YW-14 decreases by \sim 10 fold.

Fluorescence Imaging of Amyloid Plaques in 5xFAD Mouse Brain Sections. Ex vivo mouse brain section staining

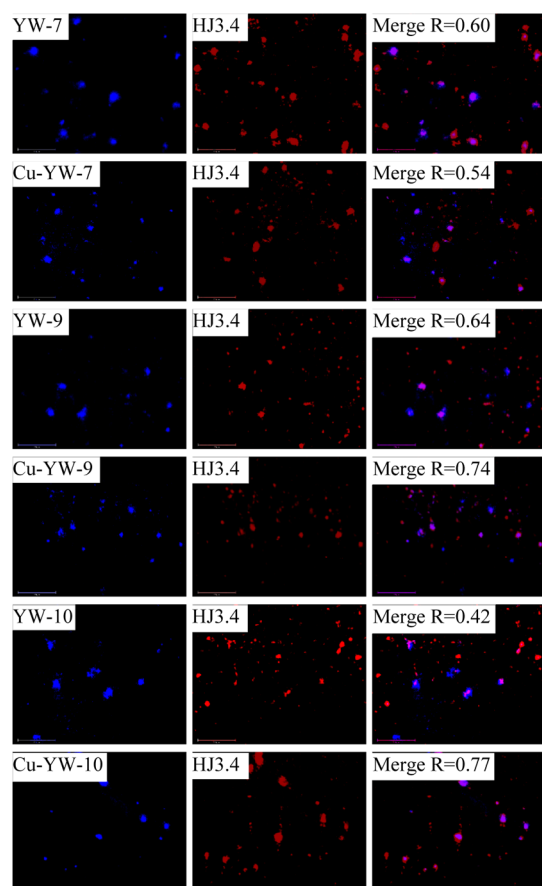


Figure 4. Fluorescence microscopy images of 5xFAD mouse brain sections incubated with YW-7, YW-9, and YW-10 as well as their Cu(II) complexes (left panels), AF594-HJ3.4 (middle panels), and merged images (right panels). The fluorescence signals from BFCs or Cu(II) complexes and the AF594-HJ3.4 antibody were monitored at 447 and 628 nm upon excitation 357 and 585 nm, respectively. Magnification: 20 \times . Scale bar: 125 μ m.

was performed to evaluate each BFC's affinity toward $A\beta$ species. Brain sections were collected from 11 month old 5xFAD mice. An appreciable amount of fluorescence intensity was observed upon incubation of the brain sections for 30 min with 50 μ M solutions of the BFCs (Figure 2, left panels). The specific staining of amyloid plaques was confirmed by staining with Congo Red (CR), another commonly used amyloid-binding fluorescent dye (Figure 2, middle panels). The fluorescent properties of BFCs indicate they exhibit labeling signal in the DAPI channel, which does not interfere with the CR signal in the Texas Red channel. The labeling ability of Cu(II) complexes was also probed using mouse brain sections of the same age. Compared to BFCs, the colocalization of the Cu(II) complexes' signal with the CR signal is improved, as indicated by Pearson's coefficients, and especially for YW-7, YW-9, and YW-10 (Figure 3). The other BFCs and their Cu(II) complexes also show moderate staining of amyloid aggregates (Figure S6). Overall, these ex vivo amyloid binding studies suggest that the BFCs show specific binding toward $A\beta$ species (see below).

The fluorescently labeled HJ3.4 antibody was utilized to confirm BFCs and their Cu(II) complexes bind specifically to the amyloid plaques (Figure 4). The HJ3.4 antibody (AF594-HJ3.4) was shown previously to bind to a range of $A\beta$ species, including $A\beta$ oligomers.^{21,34,35,45–47} Six month old 5xFAD

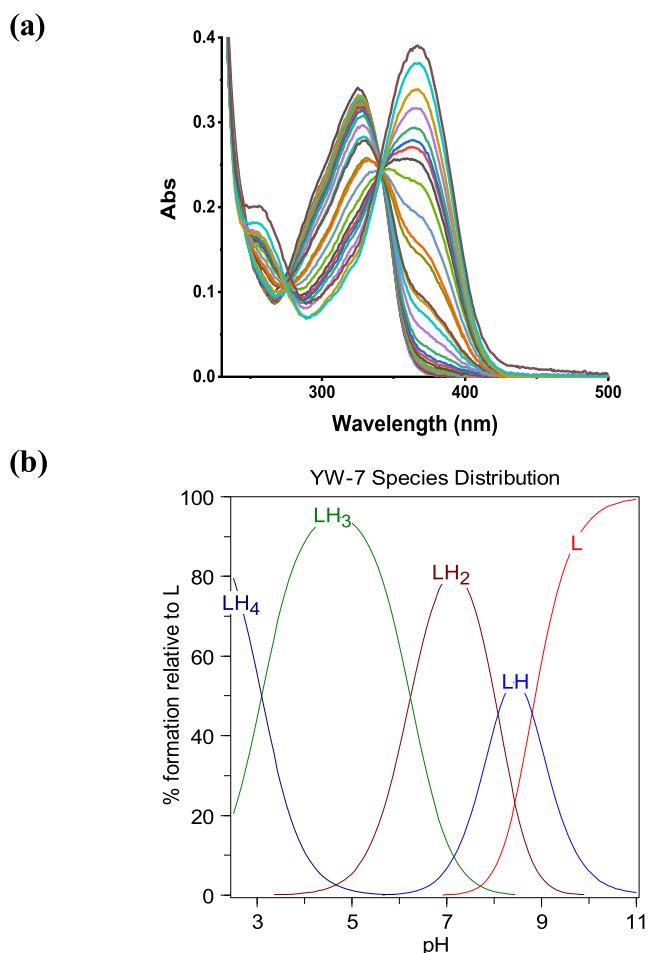


Figure 5. (a) Variable pH (pH 2.8–11.0) UV–vis spectra of YW-7 ($[L] = 20 \mu$ M, 25 $^{\circ}$ C, $I = 0.1$ M NaCl) and (b) species distribution plot.

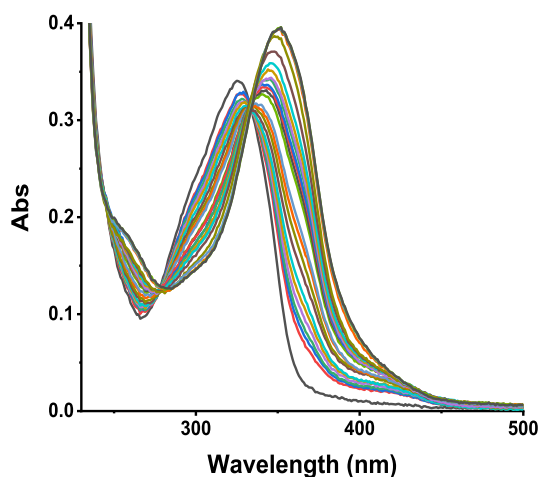
mouse brain sections were used to evaluate the BFC binding affinities, and an appreciable fluorescence intensity was observed upon treatment of brain sections for 1 h with 50 μ M solutions of the BFCs or their corresponding Cu(II) complexes. While the AF594-HJ3.4 antibody exhibits larger staining spots for the amyloid aggregates compared to Congo Red, our BFCs and their Cu(II) complexes still show favorable colocalization with AF594-HJ3.4, as suggested by the calculated Pearson's coefficients, and especially for YW-7, YW-9, and YW-10 (Figure 4). While the other BFCs and their Cu(II) complexes also show good staining of amyloid aggregates (Figure S7), overall the extent of colocalization is less for HJ3.4 than for CR because the former binds to a wide range of soluble and insoluble $A\beta$ species.

Acidity Constants of the BFCs and Stability Constants of their Cu(II) Complexes. Because all BFCs contain several acidic and basic functional groups, their acidity constants (pK_a) were determined by UV–vis spectrophotometric titrations. For YW-7, UV–vis titrations from pH 2.8 to 11.0 reveal several changes in the spectrum such as the disappearance of the band at 325 nm and the increase of the band at 367 nm with an isosbestic point at 341 nm (Figure 5a). The best fit to the data was obtained with four pK_a values: 3.09(6), 6.23(4), 8.08(2), and 8.81(1) (Table 1). Based on previously reported acidity constants for phenols and amines,^{19,43} we assigned the three lower pK_a values to the deprotonation of the amine groups of

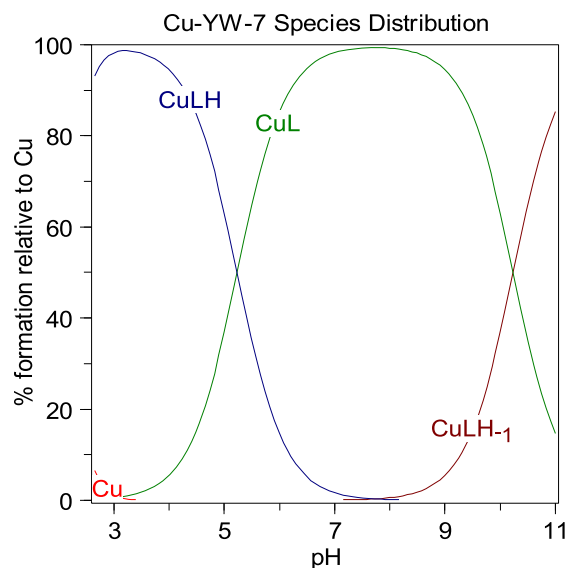
Table 1. Acidity Constants (pK_a) of YW-6 to YW-14 Determined by Spectrophotometric Titrations (Errors are for the Last Digit)

reaction	YW-6	YW-7	YW-8	YW-9	YW-10	YW-14
$[H_5L]^{4+} = [H_4L]^{3+} + H^+$ (pK_{a1})	4.15(3)	3.09(6)	3.14(4)	2.60(4)	3.40(7)	1.37(8)
$[H_4L]^{3+} = [H_3L]^{2+} + H^+$ (pK_{a2})	6.60(3)	6.23(4)	5.49(3)	5.00(3)	6.26(6)	4.53(7)
$[H_3L]^{2+} = [H_2L]^+ + H^+$ (pK_{a3})	7.93(2)	8.08(2)	8.50(3)	8.30(1)	8.32(5)	6.18(6)
$[H_2L]^+ = [HL] + H^+$ (pK_{a4})	9.90(1)	8.81(1)	10.19(2)	9.49(1)	10.43(4)	8.43(5)
$[HL] = [L]^- + H^+$ (pK_{a5})						9.87(3)

(a)



(b)

**Figure 6.** (a) Variable pH (pH 3–11) UV–vis spectra of YW-7 and the Cu(II) system ($[L] = 20 \mu M$, $[Cu^{2+}] = 18 \mu M$, $25^\circ C$, $I = 0.1 M$ NaCl) and (b) species distribution plot.

TACN, and the highest pK_a value to the phenol deprotonation. The other ester-containing BFCs show similar values to those

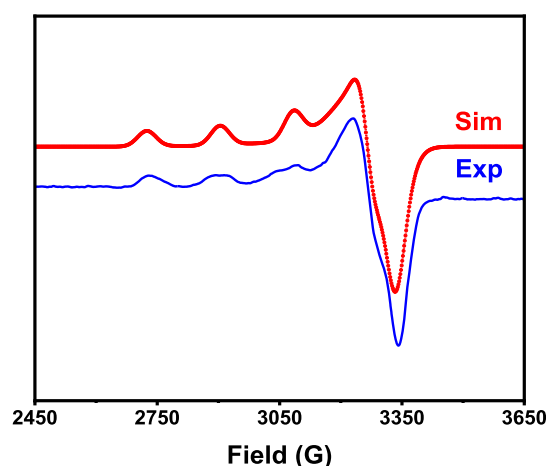
Table 2. Stability Constants ($\log K$) of the Cu(II) Complexes of YW-6 to YW-14

reaction	YW-6	YW-7	YW-8	YW-9	YW-10	YW-14
$M^{2+} + [H_2L]_+ = [MH_2L]^{3+}$						3.36(1)
$M^{2+} + HL = [MHL]^{2+}$	5.04(4)	5.24(5)	4.55(3)	5.26(2)	4.59(1)	4.55(1)
$M^{2+} + L^{-1} = [ML]^+$	16.92(4)	19.50(4)	18.47(2)	18.88(2)	17.36(1)	20.92(1)
$[ML(H_2O)]^+ = [ML(OH)] + H^+$	12.33(3)	9.26(5)	10.39(4)	10.45(4)	11.09(1)	

Table 3. Calculated pM ($-\log[M]_{free}$; $M = Cu^{2+}$) Values for a Solution Containing a 1:1 Metal/Ligand Mixture ($[M^{2+}]_{tot} = [Ligand]_{tot} = 50 \mu M$)

	YW6	YW7	YW8	YW9	YW10	YW14	DTPA ^a
pH 6.6	7.8	10.0	8.6	9.3	8.2	9.9	9.7
pH 7.4	8.7	10.8	9.5	10.1	9.4	10.8	10.7

^aDiethylenetriaminepentaacetic acid (DTPA).⁴⁸

**Figure 7.** Experimental and simulated EPR spectra of the Cu-YW-7 complex in a 1:1 PBS/glycerol glass at 77 K. The following parameters were used for the simulation: $g_z = 2.252$, A_z (Cu) = 165 G, $g_y = 2.075$, and $g_x = 2.045$.**Table 4.** Molecular Weights (MWs) of Ligands YW-7 to YW-14, and Measured $\log D_{oct}$ Values for the Corresponding ^{64}Cu Complexes

ligand	MWs ($g \cdot mol^{-1}$)	$\log D_{oct}$ (^{64}Cu complexes)
YW-7	526.7	1.26 \pm 0.02
YW-8	512.7	1.07 \pm 0.05
YW-9	498.6	1.01 \pm 0.05
YW-10	484.6	0.91 \pm 0.02
YW-14	470.6	1.15 \pm 0.02

obtained for YW-7 (Table 1). In addition, YW-14, which contains a carboxylic acid arm instead of an ester, was probed from pH 1.75 to 11.0 and the best fit was obtained with five pK_a values: 1.37(8), 4.53(7), 6.18(6), 8.43(5), and 9.87(3)

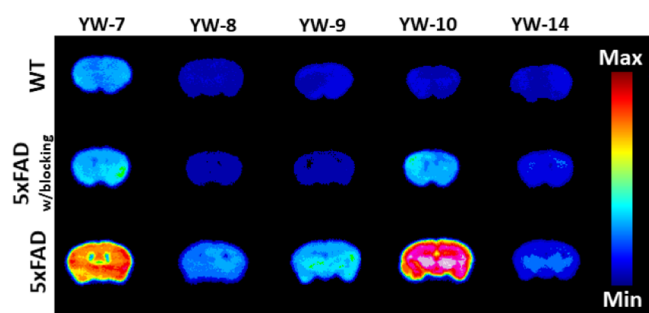


Figure 8. Autoradiography images of brain sections of WT and 5x FAD mice treated with ^{64}Cu -labeled YW-7 to YW-14, in the absence and presence with a known $\text{A}\beta$ specific blocking agent.

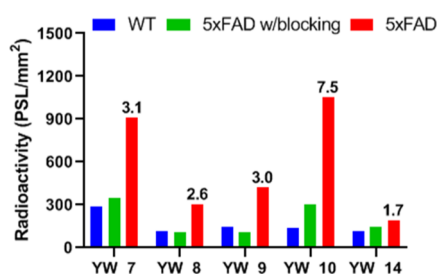


Figure 9. Average radioactivity of the brain sections in the autoradiography images. The numbers in the bar graph are the intensity ratios of 5x FAD to WT in each group.

(Table 1). Apart from the higher $\text{p}K_{\text{a}}$ values that can be assigned in a similar manner to the other BFCs, the lowest $\text{p}K_{\text{a}}$

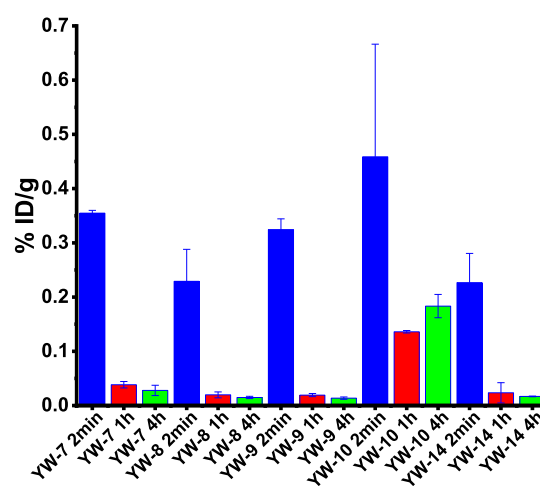


Figure 10. Brain uptake (% ID/g) results from the in vivo biodistribution study in CD-1 mice, at 2, 60, and 240 min postinjection.

value can be assigned to the deprotonation of the carboxylic acid group.

In order to quantify the metal chelation ability of the BFCs, we performed spectrophotometric titrations of ligands in the presence of $\text{Cu}(\text{II})$. To ensure full chelation of $\text{Cu}(\text{II})$ by the BFC, 0.9 equiv of $\text{Cu}(\text{ClO}_4)_2 \cdot 6\text{H}_2\text{O}$ was added. In the case of **Cu-YW-7**, the band at 325 nm disappears and the band at 352 nm rises when pH value increases, generating an isosbestic point at 333 nm (Figure 6a). The $\text{p}K_{\text{a}}$ values of the ligands and the deprotonation of a metal-bound water molecule were included in the calculation. The stoichiometry of the $\text{Cu}(\text{II})$ –

Table 5. Overall Biodistribution Results of ^{64}Cu -Labeled YW-7, YW-8, YW-9, YW-10, and YW-14 for the Three Time Points Evaluated (2, 60, and 240 min; % Injected Dose per Gram, Mean \pm SEM)

	^{64}Cu -YW-7 2 min	^{64}Cu -YW-7 1 h	^{64}Cu -YW-7 4 h	^{64}Cu -YW-8 2 min	^{64}Cu -YW-8 1 h	^{64}Cu -YW-8 4 h
blood	7.82 \pm 2.26	0.39 \pm 0.03	0.16 \pm 0.03	4.58 \pm 1.63	0.16 \pm 0.04	0.07 \pm 0.01
lung	4.96 \pm 1.12	1.77 \pm 0.98	0.76 \pm 0.18	3.48 \pm 0.52	0.47 \pm 0.11	0.34 \pm 0.04
liver	33.48 \pm 22.54	5.08 \pm 1.13	2.56 \pm 0.67	44.48 \pm 3.47	4.21 \pm 2.21	0.83 \pm 0.13
kidney	10.13 \pm 6.75	2.81 \pm 0.76	1.52 \pm 0.67	9.93 \pm 1.69	1.42 \pm 0.44	0.59 \pm 0.12
muscle	0.75 \pm 0.40	0.10 \pm 0.01	0.05 \pm 0.01	0.84 \pm 0.06	0.05 \pm 0.02	0.03 \pm 0.00
brain	0.35 \pm 0.01	0.04 \pm 0.01	0.03 \pm 0.01	0.23 \pm 0.06	0.02 \pm 0.01	0.01 \pm 0.00
bone	1.18 \pm 0.36	0.15 \pm 0.02	0.14 \pm 0.08	0.98 \pm 0.05	0.13 \pm 0.06	0.04 \pm 0.02
tail	8.84 \pm 10.15	3.34 \pm 2.70	2.59 \pm 3.43	7.33 \pm 6.22	1.99 \pm 2.49	0.16 \pm 0.04
	^{64}Cu -YW-9 2 min	^{64}Cu -YW-9 1 h	^{64}Cu -YW-9 4 h	^{64}Cu -YW-10 2 min	^{64}Cu -YW-10 1 h	^{64}Cu -YW-10 4 h
blood	5.08 \pm 0.79	0.17 \pm 0.03	0.07 \pm 0.01	11.57 \pm 2.40	1.27 \pm 0.07	0.98 \pm 0.08
lung	5.05 \pm 0.55	0.47 \pm 0.02	0.41 \pm 0.08	6.87 \pm 1.62	3.86 \pm 0.25	5.19 \pm 0.79
liver	84.61 \pm 7.49	4.11 \pm 0.64	0.84 \pm 0.07	39.82 \pm 5.59	21.81 \pm 1.36	15.61 \pm 2.81
kidney	16.31 \pm 3.42	1.95 \pm 0.57	0.60 \pm 0.08	31.04 \pm 5.04	14.18 \pm 3.38	7.49 \pm 1.54
muscle	1.02 \pm 0.16	0.06 \pm 0.00	0.02 \pm 0.01	1.83 \pm 0.56	0.56 \pm 0.16	0.39 \pm 0.06
brain	0.32 \pm 0.02	0.02 \pm 0.00	0.01 \pm 0.00	0.46 \pm 0.21	0.14 \pm 0.00	0.18 \pm 0.02
bone	1.54 \pm 0.12	0.10 \pm 0.02	0.06 \pm 0.00	2.17 \pm 0.75	0.75 \pm 0.03	0.83 \pm 0.15
tail	3.33 \pm 0.84	1.00 \pm 0.27	0.15 \pm 0.08	4.94 \pm 4.72	1.57 \pm 0.06	0.89 \pm 0.20
		^{64}Cu -YW-14 2 min		^{64}Cu -YW-14 1 h		^{64}Cu -YW-14 4 h
blood		5.59 \pm 0.86		0.10 \pm 0.04		0.06 \pm 0.02
lung		4.18 \pm 0.52		0.21 \pm 0.03		0.25 \pm 0.16
liver		51.90 \pm 2.35		1.74 \pm 0.49		0.44 \pm 0.15
kidney		11.74 \pm 1.16		1.28 \pm 1.03		0.39 \pm 0.16
muscle		0.95 \pm 0.24		0.04 \pm 0.01		0.03 \pm 0.02
brain		0.23 \pm 0.05		0.02 \pm 0.02		0.02 \pm 0.00
bone		1.08 \pm 0.26		0.06 \pm 0.02		0.06 \pm 0.02
tail		3.85 \pm 1.51		5.90 \pm 5.41		2.60 \pm 2.11

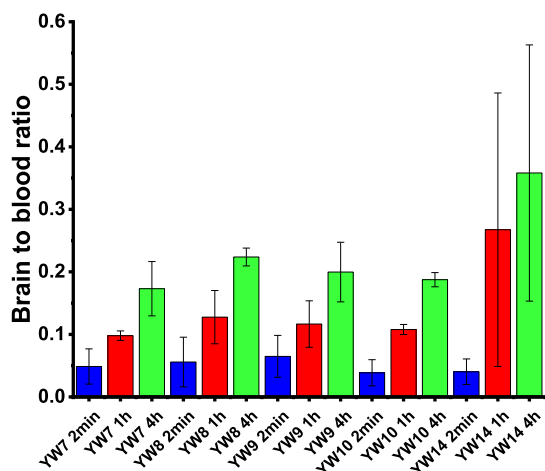


Figure 11. Brain to blood ratio results from the in vivo biodistribution study in CD-1 mice, at 2, 60, and 240 min postinjection.

BFC complexes in solution was determined by Job's plot analysis, and for Cu-YW-6 to Cu-YW-10, the breaks in the plots occur in between 0.33 and 0.5 Cu mole fraction, suggesting the formation of both 1:1 and 2:1 BFC/Cu(II) complexes in PBS (Figures S18–S22), while for Cu-YW-14 a break at ~ 0.5 Cu mole fraction suggests the formation of a 1:1 complex (Figure S23). However, when the fits for the stability constant determination included the CuL_2 species, the species distribution plots showed that the CuL_2 species formed in maximum 10% at basic pH values (Figures S24–S29). Thus, in order to perform a direct comparison of the Cu affinity for the different BFCs, and given that all ex vivo and in vivo experiments were performed with 1:1 Cu/BFC mixtures, we decided to determine the stability constants for the Cu–BFCs complexes assuming the appreciable formation of only the 1:1 Cu/BFC species.

The calculated stability constants for the various Cu/BFC species reveal that the Cu(II) complex of YW-7 exhibits a stability constant that is ~ 3 orders of magnitude larger than that of YW-6 (Table 2), which is expected given the presence of an additional metal-chelating acetate arm. In addition, Cu-YW-7 has the highest log K value (~ 19.5) among the four carboxylate ester BFCs. Interestingly, the log K value of Cu-YW-7 is only about 1 order of magnitude lower than the log K value of 20.92 for Cu-YW-14, suggesting that having a BFC with an carboxylate ester arm instead of a carboxylic acid arm does not dramatically lower the stability constant for the corresponding Cu(II) complex.

The species distribution plot of the Cu-YW-7 system was obtained based on the calculated stability constants (Figure 6b), to reveal that the concentration of free Cu(II) with YW-7 is negligible above pH 3.5, while the main species at physiological pH is the 1:1 Cu/YW-7 species with the BFCs in the monodeprotonated state. The concentrations of free Cu(II) ($\text{pM} = -\log[M_{\text{unchelated}}]$) at a specific pH value and the total ion concentration can be calculated from the solution speciation diagrams, and these pM values could be used as a direct estimate of the ligand–metal affinity and a comparison of the metal affinity among different ligands (Table 3).^{43,48,49} As such, the calculated pCu values for YW-7 and YW-14 are both 10.8 at pH 7.4, comparable to the value of 10.7 at pH 7.4 for the strong chelating agent DTPA (diethylenetriaminepenta-

acetic acid), indicating that our BFCs have a high Cu(II) binding affinity.^{43,48,49}

EPR Spectra of Cu(II) Complexes. To further characterize the Cu(II)–BFC complexes, their X-band EPR spectra were recorded in frozen glasses at 77 K. The Cu(II) complexes were prepared right before the EPR experiment by reacting the BFC with 0.8 equiv $\text{CuCl}_2 \cdot 2\text{H}_2\text{O}$. The EPR spectrum of Cu-YW-7 in a 1:1 (v/v) PBS/glycerol glass reveals a pseudoaxial EPR pattern with three different g values: $g_z = 2.252$, $A_z(\text{Cu}) = 165$ G, $g_y = 2.075$, and $g_x = 2.045$ (Figure 7). The EPR spectrum of Cu-YW-14 was also obtained similarly and exhibits a similar EPR pattern with $g_z = 2.240$, $A_z(\text{Cu}) = 168$ G, $g_y = 2.085$, and $g_x = 2.030$ (Figure S30). A different solvent system was also applied to study the Cu(II) complexes in a nonaqueous environment using 1:3 (v/v) acetonitrile/butyronitrile glass solution, and Cu-YW-7 shows a similar pattern to that in an aqueous solution (Figure S31). Finally, the EPR spectra for the Cu(II) complexes of YW-8, YW-9, and YW-10 were also collected in 1:3 (v/v) MeCN/PrCN glass, to reveal similar pseudoaxial patterns (Figures S32–S34). While the EPR spectra suggest that more than one species may be present in solution, possibly a 1:1 and a 1:2 Cu/BFC species, based on spectrophotometric titrations the 1:2 species would not be present in more than 10% under radiochemical or physiological conditions (see above).

Radiolabeling and Log D_{oct} Value Determination. The radiolabeling of compounds YW-7 to YW-14 was performed using $^{64}\text{CuCl}_2$ and employing the conditions described in the experimental section. The novel chelators were readily labeled with ^{64}Cu under mild conditions. Quality control assays were conducted using HPLC and/or TLC, and HPLC retention times were observed in the range of 9.1–9.5 min for the ^{64}Cu -radiolabeled complexes (Figure S35). All radiochemical purities were $>95\%$ within minutes at 45 °C, with specific activities of 100 Ci/mmol or greater. The UV–vis traces at 254 nm of the radio-HPLC chromatograms were also collected for the ^{64}Cu -labeled complexes, confirming that the radioactivity is due to the ^{64}Cu complexes (Figure S36). Therefore, all radiolabeled complexes were used directly without further purification.

One important aspect of developing an imaging agent for AD is that it should be able to effectively cross the BBB. To determine the hydrophobicity of the radiolabeled compounds, octanol/PBS partition coefficient values log D_{oct} were determined for ^{64}Cu complexes of YW-7 to YW-14 (Table 4). A decreasing trend of log D_{oct} values with less bulky alkyl groups was observed. Gratifyingly, the obtained log D_{oct} values for ^{64}Cu -radiolabeled complexes YW-7 to YW-14 are in the range of 0.91–1.26, which suggest their potential ability to cross the BBB.³⁸ Interestingly, the ^{64}Cu complex of YW-14, which does not contain the alkyl ester group, has a positive log D_{oct} value of 1.15 ± 0.02 and thus is likely to cross the BBB. The carboxylic acid group is normally not favorable for molecules designed to pass BBB due to its hydrophilicity. We propose the chelation of the carboxylic acid group in YW-14 with the Cu(II) center generates a neutral complex and, therefore, is beneficial for BBB penetration. We are aware that compounds with slightly higher log D_{oct} values (ideally larger than 1) would be desirable, thus we chose YW-7, YW-8, YW-9, YW-10, and YW-14 for the further characterization including autoradiography and biodistribution studies.

Autoradiography Studies. Ex vivo autoradiography studies using brain sections of 11 month old 5xFAD and

aged-matched WT mice were conducted to determine the specific binding of the ^{64}Cu -labeled BFCs to the amyloid plaques. The brain sections were stained, washed, and imaged as described in the experimental section. By comparing with the WT brain sections that show a limited background intensity (Figure 8, first row), an increased autoradiography intensity was observed upon treatment of the 5xFAD mouse brain sections with the ^{64}Cu -labeled complexes of YW-7 to YW-14 (Figure 8, third row). The specific binding to amyloid plaques of the radiolabeled BFCs was further confirmed by blocking the brain sections with the nonradioactive blocking agent 2-(4-hydroxyphenyl)benzothiazole (B_1 , Figure S37),^{19,25} which led to a remarkably decreased autoradiography intensity (Figure 8, second row). Except for YW-7 that exhibits a slight degree of nonspecific binding, the other BFCs all showed a significantly more intense signal for the 5xFAD mouse sections than the WT mouse sections. The ratios of average radioactivity of 5xFAD over WT sections are shown in Figure 9. Notably, ^{64}Cu -YW-10 exhibits a 7.5 intensity ratio of AD mouse section staining to WT sections. Due to the low signal intensity of ^{64}Cu -YW-14, more radioactivity (35 μCi) was applied in additional experiments and the difference between WT sections and AD sections is more obvious (Figure S38), although ^{64}Cu -YW-14 exhibits the least specific amyloid-binding ability among all BFCs, likely due to the neutral nature of this complex. Overall, these autoradiography results strongly suggest that the ^{64}Cu -labeled BFCs YW-7 to YW-14 exhibit the ability to detect $A\beta$ species ex vivo, and esters YW-7 to YW-10 show more specific binding to $A\beta$ plaques than acid YW-14.

Biodistribution Studies. Encouraged by the promising in vitro results, in vivo biodistribution experiments were then performed to investigate the pharmacokinetics of ^{64}Cu -YW-7 to ^{64}Cu -YW-14 complexes using CD-1 mice. The retention and accumulation of the ^{64}Cu -radiolabeled complexes in selected organs was evaluated at 2, 60, and 240 min after tracer administration (Table 5). Excitingly, appreciable brain uptake was observed for all BFCs at 2 min postinjection, followed by a rapid washout from the WT brains (Figure 10). Among all BFCs tested, ^{64}Cu -YW-10 showed the highest brain uptake of $0.46 \pm 0.21\%$ ID/g at 2 min postinjection, which dropped to $\sim 0.15\%$ ID/g at 60 min and 240 min. ^{64}Cu -YW-7 also exhibits good brain uptake of $0.35 \pm 0.01\%$ ID/g at 2 min postinjection (Table 5). The brain to blood ratio results suggest the complex retention in brain slightly increases with time, possibly due to their favorable lipophilicity (Figure 11). The small difference between the esters and carboxylic acid performance might result from the hydrolysis of the ester groups, generating a stable ^{64}Cu complex with a carboxylic acid arm, that is, ^{64}Cu -YW-14. Overall, these biodistribution studies suggest that the ^{64}Cu -radiolabeled BFCs have some brain uptake, and thus could serve as PET imaging agents for detection of $A\beta$ aggregates in vivo. While a recent study has showed that even ^{64}Cu acetate exhibits appreciable brain uptake, the blood uptake is also high in that case, and a longer early-phase clearance from blood and other organs was observed, suggesting the free ^{64}Cu might bind nonspecifically to various biomolecules.⁵⁰ Importantly, the rapid clearance from the brain suggests that these radiolabeled BFCs do not release ^{64}Cu ions in the brain to an appreciable extent, and thus should not lead to a significant background PET signal in age-matched WT controls.

CONCLUSIONS

In summary, we have successfully synthesized five BFCs YW-7 to YW-14 via linking the amyloid-targeting 2-(4-hydroxyphenyl) benzothiazole fragment with a strong metal chelator TACN, and the resulting BFCs could be radiolabeled with ^{64}Cu for PET imaging purposes. Spectrophotometric titrations were used to obtain stability constants ($\log K$'s) for the Cu(II) complexes, and the results show that adding a carboxylic acid or ester arm to the TACN fragment increases the $\log K$ for the corresponding Cu(II) complexes by 3–4 orders of magnitude versus the parent TACN derivative. Importantly, the carboxylate ester BFCs exhibit the appropriate lipophilicity and Cu-chelating ability to be potentially used in in vivo applications. The evaluation of the $A\beta$ -binding affinity for these BFCs and their ^{64}Cu complexes was probed by ex vivo AD mouse brain section fluorescence imaging and autoradiography studies. These results reveal that the Cu complexes of the carboxylate ester BFCs bind more specifically to the amyloid plaques than the Cu complex of the carboxylic acid BFC YW-14, with the *t*-butyl and methyl ester derivatives YW-7 and YW-10, respectively, showing the highest specificity. The ^{64}Cu -radiolabeled BFCs also exhibit favorable $\log D_{\text{oct}}$ values around 1, suggesting they should be BBB permeable. Finally, the in vivo biodistribution studies using the ^{64}Cu -BFC complexes reveal that they exhibit some brain uptake in CD-1 mice. Overall, we consider that these benzothiazole-TACN BFCs can serve as lead compounds for the development of ^{64}Cu PET imaging agents for AD diagnosis.

ASSOCIATED CONTENT

Supporting Information

The Supporting Information is available free of charge at <https://pubs.acs.org/doi/10.1021/acs.inorgchem.1c02079>.

Spectrophotometric titrations; Job's plots; UV-vis and fluorescence spectra; radioHPLC chromatograms; and additional autoradiography data (PDF)

AUTHOR INFORMATION

Corresponding Authors

Buck E. Rogers – Department of Radiation Oncology, Washington University School of Medicine, St. Louis, Missouri 63108, United States; orcid.org/0000-0001-8189-1797; Email: b.rogers@wustl.edu

Liviu M. Mirica – Department of Chemistry, University of Illinois at Urbana-Champaign, Urbana, Illinois 61801, United States; Hope Center for Neurological Disorders, Washington University School of Medicine, St. Louis, Missouri 63110, United States; orcid.org/0000-0003-0584-9508; Email: mirica@illinois.edu

Authors

Yujue Wang – Department of Chemistry, University of Illinois at Urbana-Champaign, Urbana, Illinois 61801, United States

Truc T. Huynh – Department of Radiation Oncology, Washington University School of Medicine, St. Louis, Missouri 63108, United States; Department of Chemistry, Washington University, St. Louis, Missouri 63130, United States

Hong-Jun Cho – Department of Chemistry, University of Illinois at Urbana-Champaign, Urbana, Illinois 61801, United States

Yung-Ching Wang – Department of Chemistry, University of Illinois at Urbana-Champaign, Urbana, Illinois 61801, United States

Complete contact information is available at:
<https://pubs.acs.org/10.1021/acs.inorgchem.1c02079>

Notes

The authors declare no competing financial interest.

ACKNOWLEDGMENTS

This work was supported by the NIH (R01GM114588 to L.M.M.). We thank the small animal imaging facilities at Washington University School of Medicine for excellent technical assistance and the Isotope Production Group at Washington University for the production of ^{64}Cu .

REFERENCES

- (1) 2020 Alzheimer's disease facts and figures. *Alzheimer's Dementia*, **2020**, *16*, 391–460. DOI: 10.1002/alz.12068
- (2) DeTure, M. A.; Dickson, D. W. The neuropathological diagnosis of Alzheimer's disease. *Mol. Neurodegener.* **2019**, *14*, 32.
- (3) Hickey, J. L.; Lim, S.; Hayne, D. J.; Paterson, B. M.; White, J. M.; Villemagne, V. L.; Roselt, P.; Binns, D.; Cullinane, C.; Jeffery, C. M.; Price, R. I.; Barnham, K. J.; Donnelly, P. S. Diagnostic Imaging Agents for Alzheimer's Disease: Copper Radiopharmaceuticals that Target A β Plaques. *J. Am. Chem. Soc.* **2013**, *135*, 16120–16132.
- (4) Tiwari, S.; Atluri, V.; Kaushik, A.; Yndart, A.; Nair, M. Alzheimer's disease: pathogenesis, diagnostics, and therapeutics. *Int. J. Nanomed.* **2019**, *14*, 5541–5554.
- (5) De Strooper, B.; Karran, E. The Cellular Phase of Alzheimer's Disease. *Cell* **2016**, *164*, 603–615.
- (6) Savelieff, M. G.; Lee, S.; Liu, Y.; Lim, M. H. Untangling Amyloid-beta, Tau, and Metals in Alzheimer's Disease. *ACS Chem. Biol.* **2013**, *8*, 856–865.
- (7) Nam, G.; Lim, M. H. Intertwined Pathologies of Amyloid-beta and Metal Ions in Alzheimer's Disease: Metal-Amyloid-beta. *Chem. Lett.* **2019**, *48*, 951–960.
- (8) Cummings, J. L.; Morstorf, T.; Zhong, K. Alzheimer's disease drug-development pipeline: few candidates, frequent failures. *Alzheimers Res. Ther.* **2014**, *6*, 37.
- (9) Klunk, W. E.; Engler, H.; Nordberg, A.; Wang, Y.; Blomqvist, G.; Holt, D. P.; Bergström, M.; Savitcheva, I.; Huang, G.-F.; Estrada, S.; Ausén, B.; Debnath, M. L.; Barletta, J.; Price, J. C.; Sandell, J.; Lopresti, B. J.; Wall, A.; Koivisto, P.; Antoni, G.; Mathis, C. A.; Långström, B. Imaging Brain Amyloid in Alzheimer's Disease with Pittsburgh Compound-B. *Ann. Neurol.* **2004**, *55*, 306–319.
- (10) Serdons, K.; Terwinghe, C.; Vermaelen, P.; Van Laere, K.; Kung, H.; Mortelmans, L.; Bormans, G.; Verbruggen, A. Synthesis and evaluation of ^{18}F -labeled 2-phenylbenzothiazoles as positron emission tomography imaging agents for amyloid plaques in Alzheimer's disease. *J. Med. Chem.* **2009**, *52*, 1428–1437.
- (11) Choi, S. R.; Golding, G.; Zhuang, Z.; Zhang, W.; Lim, N.; Hefti, F.; Benedum, T. E.; Kilbourn, M. R.; Skovronsky, D.; Kung, H. F. Preclinical Properties of 18F-AV-45: A PET Agent for A β Plaques in the Brain. *J. Nucl. Med.* **2009**, *50*, 1887–1894.
- (12) Uzuegbunam, B. C.; Librizzi, D.; Hooshyar Yousefi, B. PET Radiopharmaceuticals for Alzheimer's Disease and Parkinson's Disease Diagnosis, the Current and Future Landscape. *Molecules* **2020**, *25*, 977.
- (13) Sedgwick, A. C.; Brewster, J. T.; Harvey, P.; Iovan, D. A.; Smith, G.; He, X.-P.; Tian, H.; Sessler, J. L.; James, T. D. Metal-based Imaging Agents: Progress towards Interrogating Neurodegenerative Disease. *Chem. Soc. Rev.* **2020**, *49*, 2886–2915.
- (14) Shokeen, M.; Anderson, C. J. Molecular Imaging of Cancer with Copper-64 Radiopharmaceuticals and Positron Emission Tomography (PET). *Acc. Chem. Res.* **2009**, *42*, 832–841.
- (15) Wadas, T. J.; Wong, E. H.; Weisman, G. R.; Anderson, C. J. Coordinating Radiometals of Copper, Gallium, Indium, Yttrium, and Zirconium for PET and SPECT Imaging of Disease. *Chem. Rev.* **2010**, *110*, 2858–2902.
- (16) Krasnovskaya, O.; Naumov, A.; Guk, D.; Gorelkin, P.; Erofeev, A.; Beloglazkina, E.; Majouga, A. Copper Coordination Compounds as Biologically Active Agents. *Int. J. Mol. Sci.* **2020**, *21*, 3965.
- (17) Fodero-Tavoletti, M. T.; Villemagne, V. L.; Paterson, B. M.; White, A. R.; Li, Q.-X.; Camakaris, J.; O'Keefe, G.; Cappai, R.; Barnham, K. J.; Donnelly, P. S. Bis(thiosemicarbazonato) Cu-64 Complexes for Positron Emission Tomography Imaging of Alzheimer's Disease. *J. Alzheimer's Dis.* **2010**, *20*, 49–55.
- (18) McInnes, L. E.; Noor, A.; Kysenius, K.; Cullinane, C.; Roselt, P.; McLean, C. A.; Chiu, F. C. K.; Powell, A. K.; Crouch, P. J.; White, J. M.; Donnelly, P. S. Potential Diagnostic Imaging of Alzheimer's Disease with Copper-64 Complexes That Bind to Amyloid-beta Plaques. *Inorg. Chem.* **2019**, *58*, 3382–3395.
- (19) Bandara, N.; Sharma, A. K.; Krieger, S.; Schultz, J. W.; Han, B. H.; Rogers, B. E.; Mirica, L. M. Evaluation of ^{64}Cu -based Radiopharmaceuticals That Target A β Peptide Aggregates as Diagnostic Tools for Alzheimer's Disease. *J. Am. Chem. Soc.* **2017**, *139*, 12550–12558.
- (20) Sharma, A. K.; Schultz, J. W.; Prior, J. T.; Rath, N. P.; Mirica, L. M. Coordination Chemistry of Bifunctional Chemical Agents Designed for Applications in (^{64}Cu) PET Imaging for Alzheimer's Disease. *Inorg. Chem.* **2017**, *56*, 13801–13814.
- (21) Cho, H.-J.; Huynh, T. T.; Rogers, B. E.; Mirica, L. M. Design of a multivalent bifunctional chelator for diagnostic (^{64}Cu) PET imaging in Alzheimer's disease. *Proc. Natl. Acad. Sci. U.S.A.* **2020**, *117*, 30928–30933.
- (22) Lim, S.; Paterson, B. M.; Fodero-Tavoletti, M. T.; O'Keefe, G. J.; Cappai, R.; Barnham, K. J.; Villemagne, V. L.; Donnelly, P. S. A copper radiopharmaceutical for diagnostic imaging of Alzheimer's disease: a bis(thiosemicarbazonato)copper(II) complex that binds to amyloid-beta plaques. *Chem. Commun.* **2010**, *46*, 5437–5439.
- (23) Hickey, J. L.; Donnelly, P. S. Diagnostic Imaging of Alzheimer's Disease with Copper and Technetium Complexes. *Coord. Chem. Rev.* **2012**, *256*, 2367–2380.
- (24) Savelieff, M. G.; Nam, G.; Kang, J.; Lee, H. J.; Lee, M.; Lim, M. H. Development of Multifunctional Molecules as Potential Therapeutic Candidates for Alzheimer's Disease, Parkinson's Disease, and Amyotrophic Lateral Sclerosis in the Last Decade. *Chem. Rev.* **2019**, *119*, 1221–1322.
- (25) Huang, Y.; Cho, H.-J.; Bandara, N.; Sun, L.; Tran, D.; Rogers, B. E.; Mirica, L. M. Metal-chelating benzothiazole multifunctional compounds for the modulation and ^{64}Cu PET imaging of A β aggregation. *Chem. Sci.* **2020**, *11*, 7789–7799.
- (26) Gomes, L. M. F.; Bataglioli, J. C.; Storr, T. Metal complexes that bind to the amyloid- β peptide of relevance to Alzheimer's disease. *Coord. Chem. Rev.* **2020**, *412*, 213255.
- (27) Joshi, T.; Kubeil, M.; Nsubuga, A.; Singh, G.; Gasser, G.; Stephan, H. Harnessing the Coordination Chemistry of 1,4,7-Triazacyclononane for Biomimicry and Radiopharmaceutical Applications. *Chempluschem* **2018**, *83*, 554–564.
- (28) De Silva, R. A.; Lears, K. A.; Chong, H.-S.; Kang, C. S.; Sun, X.; Rogers, B. E. Copper-64 radiolabeling and biological evaluation of bifunctional chelators for radiopharmaceutical development. *Nucl. Med. Biol.* **2012**, *39*, 1099–1104.
- (29) Pardridge, W. M. Molecular biology of the blood-brain barrier. *Mol. Biotechnol.* **2005**, *30*, 57–70.
- (30) Henderson, J.; Piquette-Miller, M. Blood-brain barrier: an impediment to neuropharmaceuticals. *Clin. Pharmacol. Ther.* **2015**, *97*, 308–313.
- (31) Blake, A. J.; Danks, J. P.; Li, W.-S.; Lippolis, V.; Schröder, M. Synthesis and characterisation of pendant-arm amino derivatives of 1,4,7-triazacyclononane and alkyl-bridged bis(1,4,7-triazacyclononane) macrocycles and complexation to Cu(II). *J. Chem. Soc., Dalton Trans.* **2000**, 3034–3040.

(32) Gans, P.; Sabatini, A.; Vacca, A. Determination of equilibrium constants from spectrophotometric data obtained from solutions of known pH: The program pHab. *Ann. Chim.* **1999**, *89*, 45.

(33) Alderighi, L.; Gans, P.; Ienco, A.; Peters, D.; Sabatini, A.; Vacca, A. Hyperquad simulation and speciation (HySS): A utility program for the investigation of equilibria involving soluble and partially soluble species. *Coord. Chem. Rev.* **1999**, *184*, 311.

(34) Schwetye, K. E.; Cirrito, J. R.; Esparza, T. J.; Mac Donald, C. L.; Brody, D. L. Traumatic Brain Injury Reduces Soluble Extracellular Amyloid- β in Mice: A Methodologically Novel Combined Microdialysis-Controlled Cortical Impact Study. *Neurobiol. Dis.* **2010**, *40*, 555–564.

(35) Esparza, T. J.; Wildburger, N. C.; Jiang, H.; Gangolli, M.; Cairns, N. J.; Bateman, R. J.; Brody, D. L. Soluble Amyloid-beta Aggregates from Human Alzheimer's Disease Brains. *Sci. Rep.* **2016**, *6*, 38187.

(36) Kume, M.; Carey, P. C.; Gaehle, G.; Madrid, E.; Voller, T.; Margenau, W.; Welch, M. J.; Lapi, S. E. A Semi-automated System for the Routine Production of Copper-64. *Appl. Radiat. Isot.* **2012**, *70*, 1803–1806.

(37) McCarthy, D. W.; Shefer, R. E.; Klinkowstein, R. E.; Bass, L. A.; Margeneau, W. H.; Cutler, C. S.; Anderson, C. J.; Welch, M. J. Efficient Production of High Specific Activity ^{64}Cu using a Biomedical Cyclotron. *Nucl. Med. Biol.* **1997**, *24*, 35–43.

(38) Dischino, D. D.; Welch, M. J.; Kilbourn, M. R.; Raichle, M. E. Relationship between lipophilicity and brain extraction of C-11-labeled radiopharmaceuticals. *J. Nucl. Med.* **1983**, *24*, 1030–1038.

(39) See [Supporting Information](#).

(40) Biancalana, M.; Koide, S. Molecular mechanism of Thioflavin-T binding to amyloid fibrils. *Biochim. Biophys. Acta* **2010**, *1804*, 1405–1412.

(41) Mathis, C. A.; Wang, Y.; Holt, D. P.; Huang, G.-F.; Debnath, M. L.; Klunk, W. E. Synthesis and Evaluation of ^{11}C -Labeled 6-Substituted 2-Arylbenzothiazoles as Amyloid Imaging Agents. *J. Med. Chem.* **2003**, *46*, 2740–2754.

(42) Necula, M.; Kaye, R.; Milton, S.; Glabe, C. G. Small molecule inhibitors of aggregation indicate that amyloid β oligomerization and fibrillization pathways are independent and distinct. *J. Biol. Chem.* **2007**, *282*, 10311–10324.

(43) Sharma, A. K.; Pavlova, S. T.; Kim, J.; Finkelstein, D.; Hawco, N. J.; Rath, N. P.; Kim, J.; Mirica, L. M. Bifunctional Compounds for Controlling Metal-mediated Aggregation of the $\text{A}\beta_{42}$ Peptide. *J. Am. Chem. Soc.* **2012**, *134*, 6625–6636.

(44) Lipinski, C. A.; Lombardo, F.; Dominy, B. W.; Feeney, P. J. Experimental and computational approaches to estimate solubility and permeability in drug discovery and development settings. *Adv. Drug Delivery Rev.* **2001**, *46*, 3–26.

(45) Perrin, R. J.; Fagan, A. M.; Holtzman, D. M. Multimodal Techniques for Diagnosis and Prognosis of Alzheimer's Disease. *Nature* **2009**, *461*, 916–922.

(46) Fagan, A. M.; Holtzman, D. M. Cerebrospinal fluid biomarkers of Alzheimer's disease. *Biomarkers Med.* **2010**, *4*, 51–63.

(47) Sun, L.; Sharma, A. K.; Han, B.-H.; Mirica, L. M. Amentoflavone: A Bifunctional Metal Chelator that Controls the Formation of Neurotoxic Soluble $\text{A}\beta_{42}$ Oligomers. *ACS Chem. Neurosci.* **2020**, *11*, 2741–2752.

(48) Storr, T.; Merkel, M.; Song-Zhao, G. X.; Scott, L. E.; Green, D. E.; Bowen, M. L.; Thompson, K. H.; Patrick, B. O.; Schugar, H. J.; Orvig, C. Synthesis, characterization, and metal coordinating ability of multifunctional carbohydrate-containing compounds for Alzheimer's therapy. *J. Am. Chem. Soc.* **2007**, *129*, 7453–7463.

(49) Choudhary, N.; Guadalupe Jaraquemada-Peláez, M. D.; Zarschler, K.; Wang, X.; Radchenko, V.; Kubeil, M.; Stephan, H.; Orvig, C. Chelation in One Fell Swoop: Optimizing Ligands for Smaller Radiometal Ions. *Inorg. Chem.* **2020**, *59*, 5728–5741.

(50) Andreozzi, E. M.; Torres, J. B.; Sunassee, K.; Dunn, J.; Walker-Samuel, S.; Szanda, I.; Blower, P. J. Studies of copper trafficking in a mouse model of Alzheimer's disease by positron emission

tomography: comparison of ^{64}Cu acetate and ^{64}Cu GTSM. *Metalomics* **2017**, *9*, 1622–1633.